Liu et al. Nanoscale Research Letters (2016) 11:549
DOI 10.1186/s11671-016-1764-3

Nanoscale Research Letters

NANO EXPRESS Open Access

Controllable Preparation of V_2O_5/Graphene Nanocomposites as Cathode Materials for Lithium-Ion Batteries

Yanglin Liu[1,2], Yaping Wang[1*], Yifang Zhang[1], Shuquan Liang[1] and Anqiang Pan[1*]

Abstract

Transition metal oxides and graphene composites have been widely reported in energy storage and conversion systems. However, the controllable synthesis of graphene-based nanocomposites with tunable morphologies is far less reported. In this work, we report the fabrication of V_2O_5 and reduced graphene oxide composites with nanosheet or nanoparticle-assembled subunits by adjusting the solvothermal solution. As cathode materials for lithium-ion batteries, the nanosheet-assembled V_2O_5/graphene composite exhibits better rate capability and long-term cycling stability. The V_2O_5/graphene composites can deliver discharge capacities of 133, 131, and 122 mAh g^{-1} at 16 C, 32 C, and 64 C, respectively, in the voltage range of 2.5–4.0 V vs. Li/Li^+. Moreover, the electrodes can retain 85% of their original capacity at 1C rate after 500 cycles. The superior electrochemical performances are attributed to the porous structures created by the connected V_2O_5 nanosheets and the electron conductivity improvement by graphene.

Keywords: Vanadium oxides, Reduced graphene oxide, Lithium-ion batteries, Nanosheets, Nanoparticles

Background

Rechargeable lithium-ion batteries, as one of the most important energy storage devices, have been widely used in consumer electronic devices such as cell phones, laptop computers, and hybrid electrical vehicles. However, the increasing demands for better batteries push the researchers to develop new electrode materials with improved performance including higher energy density, better rate capability, and longer lifespan [1–3].

Among the numerous cathode materials, V_2O_5 is a promising material because of its low cost, abundant resource reservation, and high-energy density [4]. However, the low ionic diffusivity (10^{-12}–10^{-13} cm^2 s^{-1}) and moderate electrical conductivity (10^{-12}–10^{-13} S cm^{-1}) limit its electrochemical performance [5]. To overcome the drawbacks, great efforts have been endeavored to fabricate nanostructured materials. To date, various V_2O_5 nanomaterials, such as nanorods [6], nanotubes [7], nanowires [5, 8], nanosheets [9, 10], nanospheres [11–13], and nanoflowers [14, 15] were reported with enhanced electrochemical performance due to the kinetics improvement for redox reactions. However, the intrinsic low electronic conductivity of V_2O_5 is still undressed. More recently, making V_2O_5 nanocomposites with conductive materials are effective for obtaining high-performance electrode materials. In particular, carbonaceous materials such as carbon nanotubes [16, 17], mesoporous carbon [18], and graphene [8, 19, 20] are of great popularity in making the nanocomposites. Among them, graphene has attracted particular interest in making nanocomposites due to its excellent physical and chemical properties, including high electronic conductivity, high surface area, and superior mechanical properties. The combination between graphene and nanomaterials can not only increase the conductivity and specific surface area of active materials but also prevent them from agglomerating upon cycling [21–23]. In the past years, vanadium oxides and graphene nanocomposites, such as VO_2@graphene [24], V_2O_3@graphene [25], and V_3O_7@graphene [26], have been successfully prepared. However, the controllable preparation of vanadium oxides on graphene nanosheets with different

* Correspondence: yapingwang@csu.edu.cn; pananqiang@csu.edu.cn
[1]School of Materials Science and Engineering, Central South University, Changsha 410083, Hunan, China
Full list of author information is available at the end of the article

structures is rarely reported, which has a big effect on the electrochemical properties.

Herein, we report the structural engineering of V_2O_5/graphene with different morphologies by a solvothermal approach with subsequent annealing in air. Vanadium precursors with nanosheet or nanoparticle morphology are controllably prepared on the surface of graphene and can be converted into V_2O_5/reduced graphene oxide nanocomposites with good structural reservation in the calcination process in air. As cathode materials for lithium-ion batteries, the nanosheet-structured V_2O_5/reduced graphene oxide nanocomposites exhibit much better rate capability and cyclic stability than V_2O_5 nanoparticles/reduced graphene oxide composites. The relationship between nanostructures and their electrochemical performance is discussed.

Methods

Materials Synthesis

The graphene oxide was made by a modified Hummers method [27]. For the composite synthesis, 10 mg dried graphene oxide (GO) nanosheets were dispersed in 30 mL of isopropyl alcohol by ultra-sonication for 30 min. Then, 0.4 mL of vanadium triisopropoxy oxide (Alfa Aesar) was added into the solution immediately. The mixture was stirred for 10 min before transferring to a 50-mL Teflon-lined stainless steel autoclave, which was later kept at 200 °C for 12 h. After cooling down naturally, the precursor precipitates were collected by centrifugation and washed several times by alcohol, before drying at 60 °C for 12 h. Finally, the dried precursor was annealed at 320 °C for 1 h in air. The obtained material was designated as nanoparticle-structured V_2O_5/reduced graphene oxide composite I (V/GO-I).

The nanoparticle-assembled V_2O_5/graphene composite was prepared by adding extra 2 mL deionized (DI) water into the solvothermal solution, keeping other parameters unaltered. The obtained material was designated as nanoparticle-structured V_2O_5/reduced graphene oxide composite II (V/GO-II).

Materials Characterization

The crystal phases were collected using a Rigaku D/max2500 with Cu-Kα radiation ($\lambda = 1.54178$ Å) using a step of 0.02° between 10° and 80° (2θ). The morphologies of the samples were studied by scanning electron microscopy (SEM, FEI Nova Nano SEM 230) and transmission electron microscopy (TEM, FEI Tecnai G20). The X-ray diffraction (XRD) patterns of the samples were collected in the range between 10° and 80° with a step size of 0.02°. The weight percentages of graphene in the V_2O_5/graphene composites were determined by thermogravimetric (TG) analysis with a heating rate of 10 °C min^{-1}. A spectrometer (Raman, LabRAM HR800) with a back-illuminated charge-coupled detector attachment was used to record the Raman spectra.

Electrochemical Measurement

The electrochemical performances of the electrodes were tested in a coin cell assembly (2016 type coin cell). For the electrode preparation, a mixture of V_2O_5/reduced graphene oxide composites, acetylene black, and polyvinylidene fluoride (PVDF) in a weight ratio of 70:20:10 was dispersed in an *N*-methyl-2-pyrrolidone (NMP) solution to make a slurry, which was coated on aluminum foil and dried in a vacuum oven at 100 °C overnight. The cells were assembled in the glove box (Mbraun, Germany) filled with ultra-high-purity argon using polypropylene membrane as the separator, lithium metal as the anode, and 1-M $LiPF_6$ in ethyl carbonate/dimethyl carbonate (1:1 *v*/*v*) as the electrolyte. The cyclic voltammetry (CV) measurement was tested on CHI660C (CH Instrument Electrochemical Workstation), and the galvanostatic discharging/charging experiment was tested on a Land battery tester (Land CT 2001A, Wuhan, China). The measurements were all carried out in the voltage range of 2.5–4.0 V (vs. Li/Li^+). The electrochemical impedance spectrometry (EIS) was carried out on a ZAHNER-IM6ex electrochemical workstation (ZAHNER Co. Germany) in the frequency range of 100 kHz to 10 mHz using the fresh cell.

Results and Discussion

Figure 1 illustrates the two different synthetic processes of V_2O_5/graphene nanocomposites with diverse self-assembled subunits. As indicated by process I, vanadium precursor nanosheets are grown on the graphene nanosheets first during the solvothermal process, in which vanadium triisopropoxy oxide ($VO(O^iPr)3$) was used as the vanadium resources. The prepared vanadium precursor and graphene composite can be converted into V_2O_5 and graphene composite with well-preserved structures. Process II indicates the preparation of nanoparticle-assembled vanadium precursor and graphene composite by adding extra 2 mL de-ion water in the solvothermal solution. Thereafter, the precursor composite can be converted into V_2O_5 nanoparticles and reduced graphene oxide nanocomposites (V/GO-II).

Figure 2a shows the SEM image of the solvothermal products from process I, which indicates the homogenous distribution of vanadium precursor on graphene nanosheets. As we know, graphene oxides have large amount of functional groups on its surface, which is helpful for the growth of vanadium precursors. The vanadium precursors are composed of nanosheets and uniformly grew on the reduced graphene oxide substrates. The vanadium precursor nanosheets are about 1 μm in-plane and connect with neighboring nanosheets to form porous structure on the

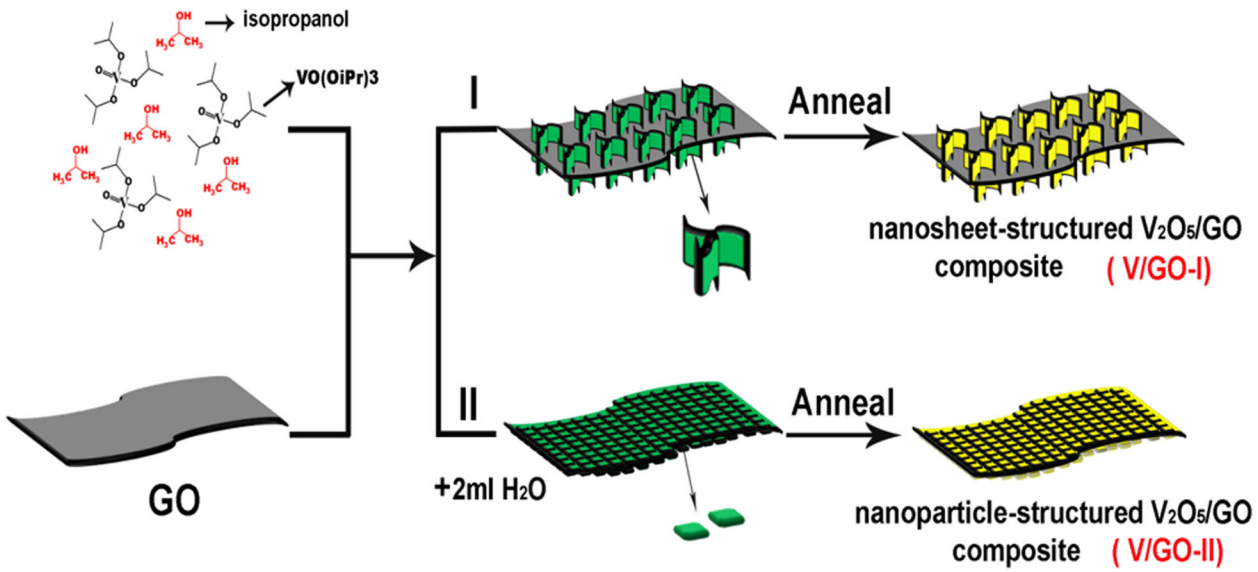

Fig. 1 Schematic illustration of preparation of V_2O_5/graphene composites with nanosheet (I) and nanoparticle (II) assembled subunits. Process I and II indicate the solvothermal synthesis using different solvent compositions

surface of graphene nanosheets. In the formation of the composite, graphene functions as a planar templates and the growth of nanosheets on its surface can greatly prevent their restacking and improve the electrolyte penetration. Figure 2b shows the FESEM image of the nanoparticle-assembled vanadium precursor and graphene composite. The vanadium precursor is of nanoparticle morphology and distributes homogeneously on the graphene nanosheets. Additional file 1: Figure S1 shows the XRD patterns of the solvothermally prepared two composites. The detection of broad XRD peaks around 30° can be attributed to the reduced graphene nanosheets. No other distinguishable XRD peaks are detected for the nanosheet-assembled vanadium precursor/GO composite, indicating the amorphous feature of the vanadium-precursor nanosheets. However, the XRD peak of the nanoparticle-assembled vanadium precursor/reduced graphene composite can be attributed to VO_2 phase (space group: *P42/mnm* (136); $a = 0.4556$ nm, $b = 0.4556$ nm, $c = 0.285$ nm, JCPDS card no. 76-0677). The formation of VO_2 phase can be attributed the reduction of $V_2O_5{\cdot}nH_2O$ by alcohol during solvothermal process, in which $V_2O_5{\cdot}nH_2O$ is prepared by the hydrolysis of vanadium triisopropoxy oxide with water. The result indicates the structures of the vanadium precursor can be adjusted by the addition of 2 mL de-ion water. The addition of water can speed the hydrolysis reaction between vanadium triisopropoxy oxide and water to form brown colored $V_2O_5{\cdot}nH_2O$, which may generate more nucleation on the graphene nanosheets, but sacrificing their parcel growth. However, due to the amorphous feature of the vanadium precursor nanosheets, it is difficult to give the exact reaction during

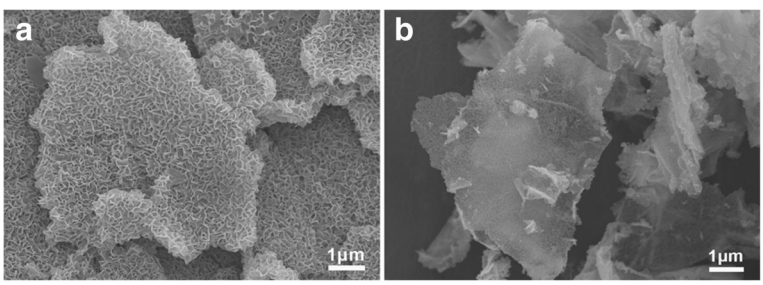

Fig. 2 SEM images of the nanosheet-assembled vanadium precursor/GO composite (**a**) and nanoparticle-assembled vanadium precursor/GO composite (**b**)

the solvothermal process. The formation of the amorphous nanosheets may be attributed to the decomposition of vanadium triisopropoxy oxide under the condition of high temperature and high pressure during the solvothermal process. Much less nuclei seeds are formed on the reduced graphene oxide and grow continuously to form the nanosheet morphology without the addition of water.

Figure 3 shows the powder X-ray diffraction (XRD) patterns of the V/GO-I composite and the V/GO-II composite. After calcination, the identified diffraction peaks can be indexed to the orthorhombic V_2O_5 phase (space group: *Pmmn* (no. 59); $a = 1.1516$ nm, $b = 0.3565$ nm, $c = 0.4372$ nm, JCPDS card no. 41-1426). The existence of reduced graphene oxides in the composite was confirmed by the Raman results, as shown in Fig. 4. The characteristic peaks at 1350 and 1580 cm^{-1} correspond to the typical G and D bands of graphene. Moreover, the intensity ratio between G and D bands become larger, indicating the partial reduction of graphene oxide. All other Raman peaks for the V/GO-I composite and the V/GO-II composite can be characterized on the basis of the vanadium oxide (Table 1) [28–30]. The weight percentage of graphene in the composite was determined by TG analysis and the result is shown in Fig. 5. The gentle weight loss before 200 °Ccan be ascribed to the evaporation of physical adsorbed water, and the fast weight drop thereafter can be attributed to the burning out of reduced graphene oxides. Therefore, the content of reduced graphene oxide in the composite is approximately 7%.

Figure 6 shows the structural characterization of the V/GO-I composite, which is obtained by annealing the nanosheet-assembled vanadium precursor and reduced graphene oxides in air. According to FESEM image (Fig. 6a), the nanosheet morphology of the vanadium precursor can be well-preserved after conversion into V_2O_5. Moreover, the existence of graphene in the composite is also demonstrated by the broken part of the composite, as shown in Fig. 6b. The result is in good accordance with the Raman and TG analysis results. The high-magnification FESEM image (Fig. 6c) shows the V_2O_5 nanosheets are unparalleled to each other to form a porous three-dimensional structure, which may be of advantage of preventing the re-stack of graphene nanosheets and the electrolyte penetration. Figure 6d shows the elemental mapping results of the nanosheet-assembled V_2O_5 and reduced graphene oxide composites,

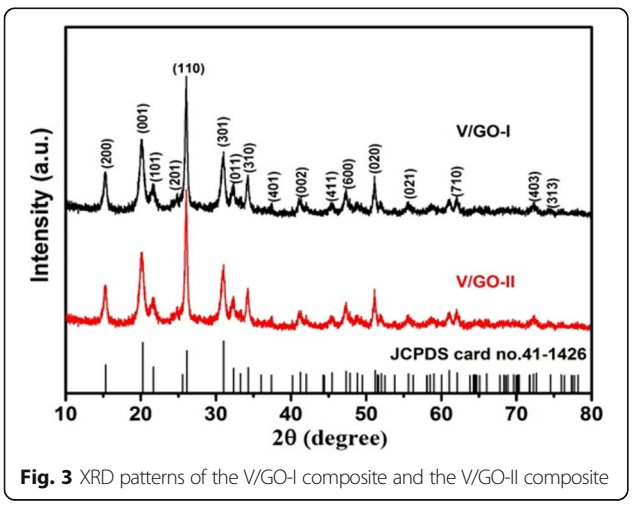

Fig. 3 XRD patterns of the V/GO-I composite and the V/GO-II composite

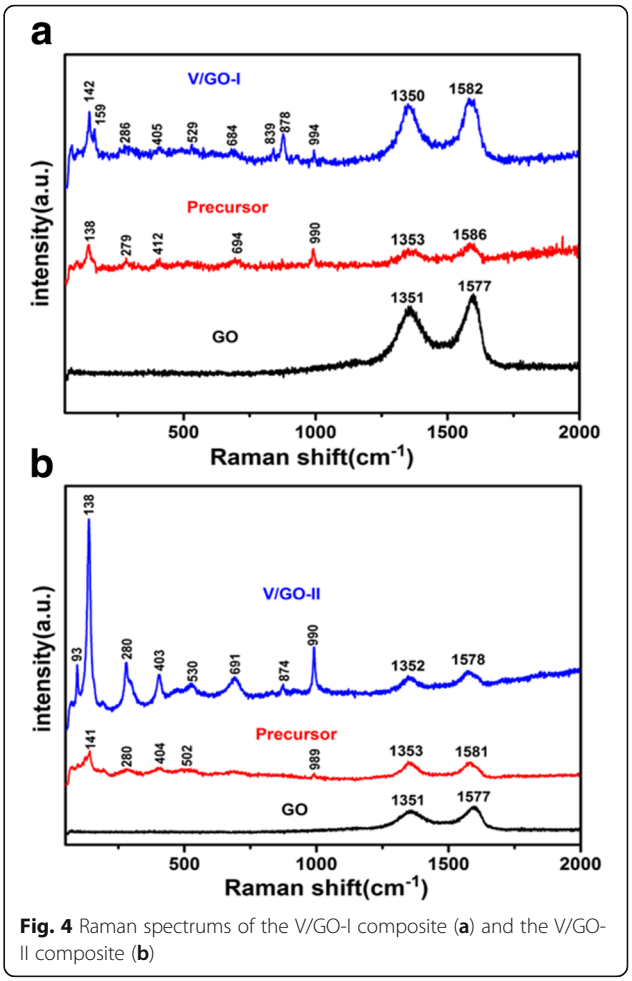

Fig. 4 Raman spectrums of the V/GO-I composite (**a**) and the V/GO-II composite (**b**)

Table 1 Raman peaks and their assignments of V_2O_5

Frequency (cm^{-1})	Assignment	Vibration modes
994	Stretching vibration of V=O	A_g
684	Stretching vibration of $V–O_1$	B_{2g} and B_{3g}
529	Stretching vibration of $V–O_2$	A_g
405	Bending vibration of $V–O_2–V$	A_g
286	Bending vibration of $O_3–V–O_2$	B_{2g}
138	Lattice vibration	B_{3g}

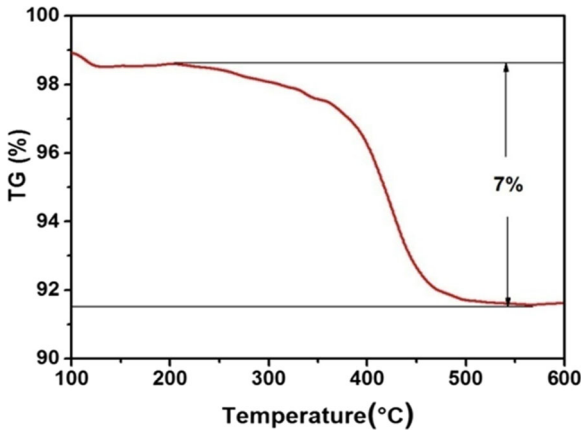

Fig. 5 TG curve of the V/GO-I composite in air from 100 to 600 °C. The temperature ramp rate was 5 °C min^{-1}

which reveals the uniform distribution of C, V, and O elements in the composite. Figure 6e, f shows the TEM images of V_2O_5 nanosheets and graphene oxide composite, indicating the porous feature of the vanadium oxides and their high uniformity.

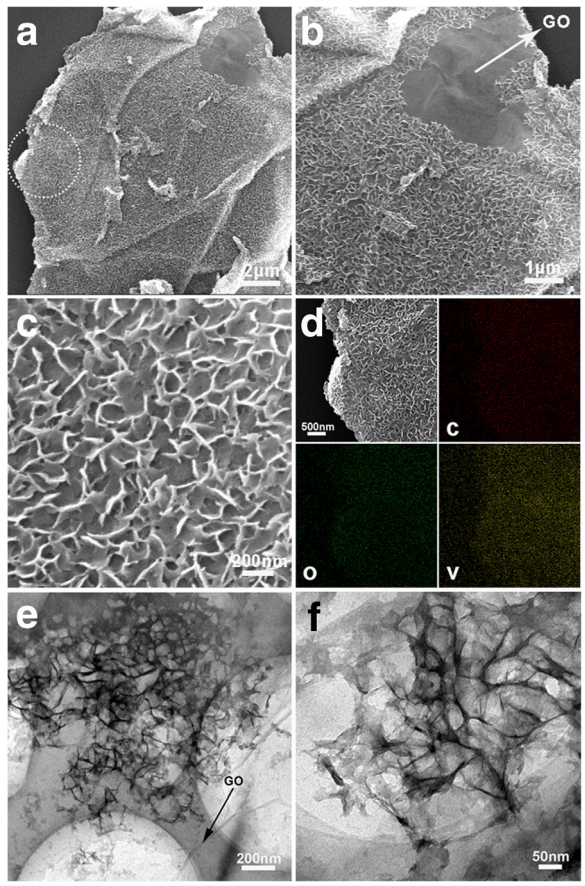

Fig. 6 SEM (**a**, **b**, **c**), elemental mapping result (**d**), and TEM images (**e**, **f**) of the V/GO-I composite at different magnifications

Figure 7 shows the FESEM and TEM images of the nanoparticle-assembled V_2O_5 and reduced graphene oxides. According to the FESEM images (Fig. 7a, b), the V_2O_5 nanoparticles in the composite is homogeneously distributed on reduced graphene oxide nanosheets, similar to the morphology of the nanoparticle-assembled vanadium precursor and reduced graphene oxide composite in Fig. 2b. The TEM images give more detailed information the structure. The nanoparticles are about 50–100 nm in-plane size. The HRTEM image (Fig. 7d) reveals the stacking feature of the nanoparticles and each nanoparticle is further composed of several closely stacked small nanosheets. Moreover, the lattice fringes are well observed with a distance of 0.576 nm, in good agreement with the planar distance of (200).

The V_2O_5 and reduced graphene oxide composites were assembled into coin cells to evaluate their electrochemical properties and the results are shown in Fig. 8. Figure 8a shows the first consecutive five CV curves for the V/GO-I composite at a scan rate of 0.1 mV s^{-1}. Two pairs of redox peaks are clearly observed for each cycle, which indicates the multiple step phase transitions for V_2O_5 and reduced graphene oxide composite. The cathodic peaks at 3.39 and 3.19 V correspond to the phase transition from V_2O_5 to ε-$Li_{0.5}V_2O_5$, then to δ-$Li_{1.0}V_2O_5$, respectively. And the two corresponding anodic peaks at 3.23 and 3.43 V are related to the phase transformations from δ-$Li_{1.0}V_2O_5$ to ε-$Li_{0.5}V_2O_5$, and then to V_2O_5 in return [31–33]. No distinct peak intensity and potential position changes for the subsequent cycles are detected, suggesting the good reversibility of

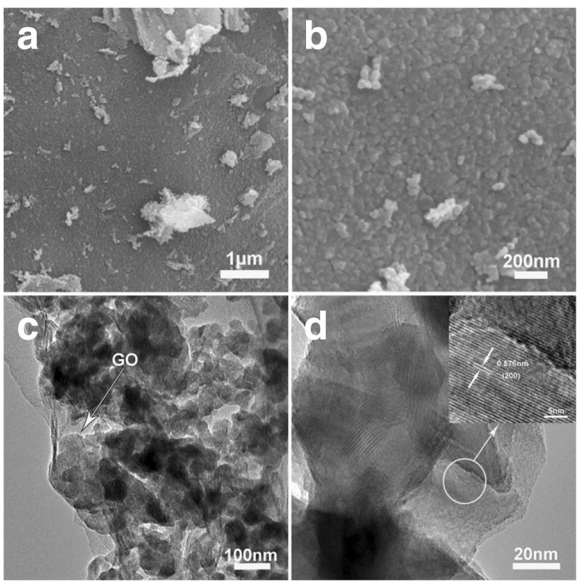

Fig. 7 SEM (**a**, **b**) and TEM (**c**, **d**) images of the V/GO-II composite. The *inset* in (**d**) shows the HRTEM image of the V/GO-II composite

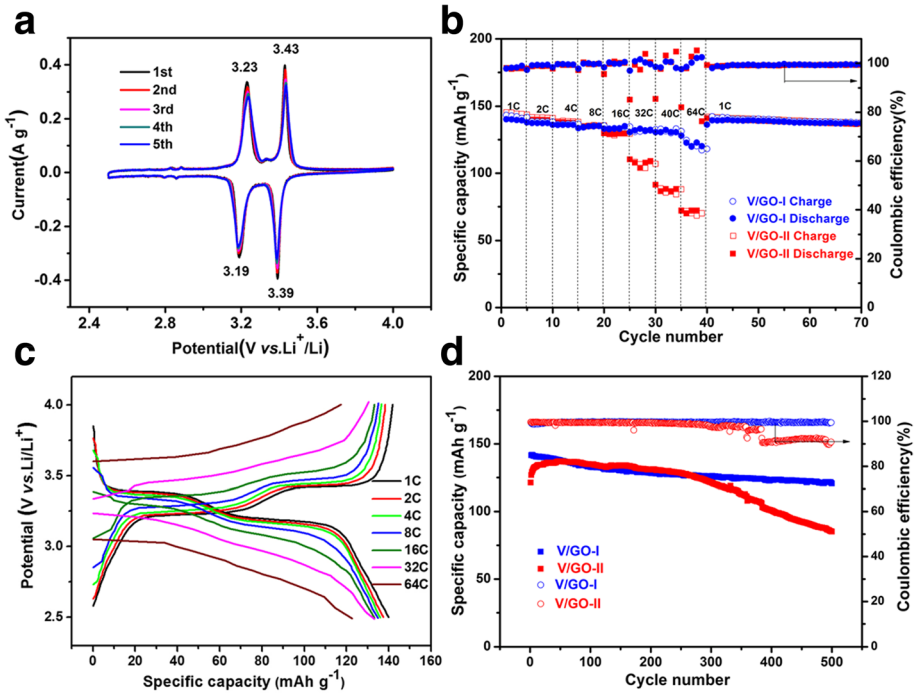

Fig. 8 **a** CV curves of the V/GO-I composite at a scan rate of 0.1 mV s^{-1}. **b** Rate capability of the V/GO-I composite and the V/GO-II composite at different current densities. **c** Discharge/charge voltage profiles of the V/GO-I composite at different current rates. **d** Cycling performance of the V/GO-I composite and the V/GO-II composite at a current rate of 2C

the electrode. Moreover, two weak redox peaks between 2.8 and 2.9 V can be detected, which may be attributed to the surface adoption or desorption of Li^+ ions upon cycling. Comparing to the CV curves for V/GO-II composite (Additional file 1: Figure S2), the V/GO-I composite exhibit higher peak intensity and smaller polarization [34].

Figure 8b shows the rate performances of the composites. Both V/GO-I and V/GO-II composite electrodes exhibit good rate capability. The capacities vary slightly for the composites less than 8C. However, the rate performance of the V/GO-I composite becomes obvious at rates higher than 16C. A specific capacity of 133 mA h g^{-1} can be obtained for V/GO-I composite even at 16C, which is very close to the theoretical capacity of 147 mA h g^{-1} for one lithium-ion intercalation per formula. Moreover, almost no capacity fade is detected at 32C and 40C. Even at 64C, the V/GO-I composite can still deliver a specific discharge capacity of 122 mAh g^{-1}. However, the capacity decreases much faster at high rates (>16C) for V/GO-II composite. The corresponding charge/discharge curves are shown in Additional file 1: Figure S3. The composite electrodes deliver specific discharge capacities of 108, 85, 74, and 50 mA h g^{-1} at 16C, 32C, 40C and 64C, respectively. When the discharge/charge rates were reset to 1C, high discharge capacity of 139 mAh g^{-1} can be recovered for both composites. The coulombic efficiency of V/GO-I composite is close to 100% in the whole discharge/charge process.

Figure 8c shows the charge/discharge profiles of the V/GO-I composite at various rates. The working potentials decrease gradually and the discharge/charge plateaus can still be observed even at higher rates. The voltage gap is much smaller and the capacity is larger than those for V/GO-II composite. The result indicates the lower polarization of the nanosheet-assembled V_2O_5/graphene composite, which may be attributed to the porous structures created by the nanosheets.

Figure 8d shows the long-term cycling performance for the two V_2O_5/graphene composites. The V/GO-I composite deliver an initial high specific capacity of 142 mAh g^{-1} at 2C and retain a capacity of 121 mA h g^{-1} after 500 cycles. The average capacity fading is only 0.03% per cycle. For comparison, the V/GO-II composite only retains a capacity of 80 mA h g^{-1} after 500 cycles at the same rate. Additional file 1: Figure S4 shows the charge/discharge profiles of the first, tenth, 100th, and 500th cycles at 2C for the two composites. As shown in Additional file 1: Figure S4a, The initial discharge and charge capacities are 142.1 and 141.6 mA h g^{-1}, respectively, for the V/GO-I composite and the coulombic efficiency can be of 99.6%. After 500 cycles, the plateaus can still be easily detected. Additional file 1: Figure S4b shows the discharge/

charge profiles for V/GO-II composite, which indicates the significant change of the plateaus for the 500th cycle. The result demonstrates the improved cycling stability of the V/GO-I composite.

Figure 9 shows the electrochemical impedance spectroscopy (EIS) measurement results for both electrodes, which acquired from fresh cells. The semi-cycle for V/GO-I is much smaller than that for V/GO-II composite. According to the simulation result, the charge transfer resistance for V/GO-I is about 55.03 Ω, which is far less than 104 Ω for the V/GO-II composite. The result demonstrates the improved charge transfer kinetics for the nanosheet-assembled V_2O_5 and reduced graphene oxide composite. According to the electrochemical analysis results, the nanosheet-assembled V_2O_5/graphene composite exhibit better rate capability, cycling stability, and lower charge transfer resistance than the nanoparticle-assembled V_2O_5/graphene composite. The electrochemical performance of V/GO-I composite is also much better than many previously reported V_2O_5 electrodes, such as hollow structured V_2O_5 microspheres [35] and three-dimensional porous V_2O_5 [36]. Table 2 lists the rate performance of V_2O_5-based electrodes in this work and from many previous reported literatures. As shown in Table 2, the nanosheet-assembled V_2O_5/r-GO composite exhibit higher capacity and better rate capability than many other V_2O_5-based electrodes. The excellent rate performance and superior cyclic stability can be attributed to the synergistic effects between V_2O_5 and graphene substrates, which include the following aspects: (1) the growth of V_2O_5 nanosheets on reduced graphene oxide can ensure the good electronic conductivity of the electrode materials; (2) the porous space created by the interconnected large nanosheets can improve the accessibility of the electrolyte with the electrode materials; (3) the ultra-thin nanosheet thickness can greatly reduce the Li^+ ions diffusion and electron transportation distances; and (4) the porous structure may better accommodate the volume changes upon cycling.

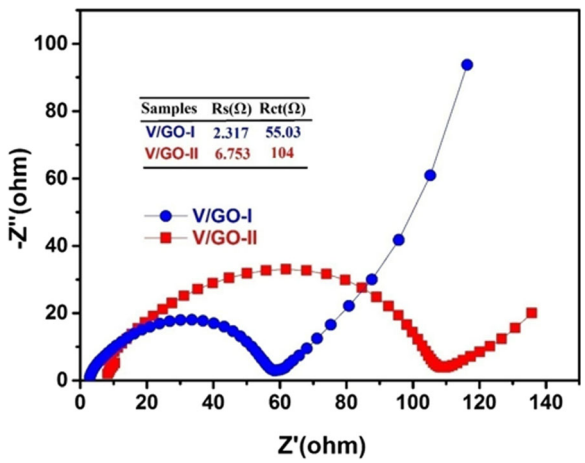

Fig. 9 Nyquist plots and the equivalent circuit model as well as the simulated results for the V/GO-I composite and the V/GO-II composite

Table 2 Electrochemical properties of V_2O_5 and its hybrid composites

Electrode description	Voltage window (V)	Current density (mA g^{-1})	Specific capacity (mA h g^{-1})
V_2O_5 nanoparticles [37]	2.5–4	147 (1C)	138
		588 (4C)	116
		1176 (8C)	88
V_2O_5 nanosheets [32]	2.5–4	200 (1.4C)	138
		3200 (21.7C)	119
V_2O_5 nanospheres [12]	2.5–4	220 (1.5C)	136
		2205 (15C)	92
V_2O_5 nanobelts [31]	2.5–4	147 (1C)	139
		1176 (8C)	127
V_2O_5 microspheres [35]	2.5–4	147 (1C)	140
		2940 (20C)	120
V_2O_5 nanoribbon [38]	1.5–3.75	43.7 (0.1C)	290
		437 (1C)	190
		874 (2C)	120
V_2O_5@carbon composite [39]	2.5–4	147 (1C)	140
		2352 (16C)	125
		4704 (32C)	122
This work	2.5–4	147 (1C)	140.2
		2352 (16C)	133
		4704 (32C)	131

Conclusions

In summary, nanosheet- or nanoparticle-assembled V_2O_5/reduced graphene oxide composites are synthesized by adjusting the solvothermal condition. The vanadium precursor can grow homogeneously on the reduced graphene oxides and the obtained composites can be converted into V_2O_5/reduced graphene oxide composites with good structural reservation. As cathode materials for lithium-ion batteries, the nanosheet-assembled V_2O_5/reduced graphene oxide nanocomposites (V/GO-I) exhibit better rate capability and cycling stability than the nanoparticle-assembled V_2O_5/graphene nanocomposites (V/GO-II). The superior electrochemical performance is attributed to the synergistic effects between V_2O_5 nanosheets and reduced graphene oxides.

Additional file

Additional file 1: XRD patterns of vanadium precursors, CV curves, charge/discharge profiles of the V@GO-II composite. Discharge/charge voltage profiles of the V@GO-I composite. Raman peaks and their

assignments of V_2O_5. Figure S1. XRD patterns of the nanosheet-assembled vanadium precursor/GO composite (blue line) and the nanoparticle-assembled vanadium precursor/GO composite (red line). Figure S2. CV curves of the V/GO-II composite at a scan rate of 0.1 mV s^{-1}. Figure S3. Charge/discharge profiles of the V@GO-II composite at different densities. Figure S4. Discharge/charge voltage profiles of the V@GO-I composite (a) and the V@GO-I composite (b) at a current rate of 2C. (DOC 4760 kb)

Abbreviations

CV: Cyclic voltammetry; FESEM: Field emission scanning electron microscopy; GO: Graphene oxide; TEM: Transmission electron microscopy; V/GO-I: Nanosheet-structured V_2O_5/reduced graphene oxide composite I; V/GO-II: Nanoparticle-structured V_2O_5/reduced graphene oxide composite II; XRD: X-ray diffraction

Acknowledgements

The financial supports by National Natural Science Foundation of China (No.51302323), Program for New Century Excellent Talents in University (NCET-13-0594), Research Fund for the Doctoral Program of Higher Education of China (No.201301621200), and Natural Science Foundation of Hunan Province, China (14JJ3018), are acknowledged. Prof. Guozhong Cao from University of Washington is acknowledged for the discussion.

Authors' Contributions

YL and YW did the most experiments in this work. YZ carried out the TG analysis. AP and YW made the research plan. SL gave some advices on the work. All authors read and approved the final manuscript.

Competing Interests

The authors declare that they have no competing interests.

Author details

[1]School of Materials Science and Engineering, Central South University, Changsha 410083, Hunan, China. [2]Changsha Environmental Protection Vocational College, Changsha 410004, Hunan, China.

Received: 21 August 2016 Accepted: 30 November 2016
Published online: 12 December 2016

References

1. Armand M, Tarascon JM (2008) Building better batteries. Nature 451:652–7
2. Wang Y, Cao G (2008) Developments in nanostructured cathode materials for high-performance lithium-ion batteries. Adv Mater 20:2251–69
3. Bruce PG, Scrosati B, Tarascon JM (2008) Nanomaterials for rechargeable lithium batteries. Angew Chem Int Ed 47:2930–46
4. Li Y, Yao J, Uchaker E, Yang J, Huang Y, Zhang M, Cao G (2013) Leaf-like V_2O_5 nanosheets fabricated by a facile green approach as high energy cathode material for lithium-ion batteries. Adv Energy Mater 3:1171–5
5. Mai L, Xu L, Han C, Xu X, Luo Y, Zhao S, Zhao Y (2010) Electrospun ultralong hierarchical vanadium oxide nanowires with high performance for lithium ion batteries. Nano Lett 10:4750–5
6. Pan A, Zhang J-G, Nie Z, Cao G, Arey BW, Li G, Liang S-Q, Liu J (2010) Facile synthesized nanorod structured vanadium pentoxide for high-rate lithium batteries. J Mater Chem 20:9193
7. Huang S-Z, Cai Y, Jin J, Li Y, Zheng X-F, Wang H-E, Wu M, Chen L-H, Su B-L (2014) Annealed vanadium oxide nanowires and nanotubes as high performance cathode materials for lithium ion batteries. J Mater Chem A 2:14099–108
8. Lee JW, Lim SY, Jeong HM, Hwang TH, Kang JK, Choi JW (2012) Extremely stable cycling of ultra-thin V_2O_5 nanowire–graphene electrodes for lithium rechargeable battery cathodes. Energy Environ Sci 5:9889
9. Rui X, Lu Z, Yu H, Yang D, Hng HH, Lim TM, Yan Q (2013) Ultrathin V_2O_5 nanosheet cathodes: realizing ultrafast reversible lithium storage. Nanoscale 5:556–60
10. Jiang Z, Lu WJ, Li ZP, Ho KH, Li X, Jiao XL, Chen DR (2014) Synthesis of amorphous cobalt sulfide polyhedral nanocages for high performance supercapacitors. J Mater Chem A 2:8603–6
11. Su DW, Dou SX, Wang GX (2014) Hierarchical orthorhombic V_2O_5 hollow nanospheres as high performance cathode materials for sodium-ion batteries. J Mater Chem A 2:11185–94
12. Wang S, Lu Z, Wang D, Li C, Chen C, Yin Y (2011) Porous monodisperse V_2O_5 microspheres as cathode materials for lithium-ion batteries. J Mater Chem 21:6365
13. Pan A, Wu HB, Yu L, Lou XW (2013) Template-free synthesis of VO_2 hollow microspheres with various interiors and their conversion into V_2O_5 for lithium-ion batteries. Angew Chem Int Ed 52:2226–30
14. Pang H, Dong Y, Ting SL, Lu J, Li CM, Kim DH, Chen P (2013) 2d single- or double-layered vanadium oxide nanosheet assembled 3D microflowers: controlled synthesis, growth mechanism, and applications. Nanoscale 5:7790–4
15. Parida MR, Vijayan C, Rout CS, Sandeep CSS, Phiip R, Deshmukh PC (2011) Room temperature ferromagnetism and optical limiting in V_2O_5 nanoflowers synthesized by a novel method. J Phys Chem C 115:112–7
16. Yu R, Zhang C, Meng Q, Chen Z, Liu H, Guo Z (2013) Facile synthesis of hierarchical networks composed of highly interconnected V_2O_5 nanosheets assembled on carbon nanotubes and their superior lithium storage properties. ACS Appl Mater Interfaces 5:12394–9
17. Sathiya M, Prakash AS, Ramesha K, Tarascon JM, Shukla AK (2011) V_2O_5-anchored carbon nanotubes for enhanced electrochemical energy storage. J Am Chem Soc 133:16291–9
18. Zhang X-F, Wang K-X, Wei X, Chen J-S (2011) Carbon-coated V_2O_5 nanocrystals as high performance cathode material for lithium ion batteries. Chem Mater 23:5290–2
19. Liu H, Yang W (2011) Ultralong single crystalline V_2O_5 nanowire/graphene composite fabricated by a facile green approach and its lithium storage behavior. Energy Environ Sci 4:4000–8
20. Rui X, Zhu J, Sim D, Xu C, Zeng Y, Hng HH, Lim TM, Yan Q (2011) Reduced graphene oxide supported highly porous V_2O_5 spheres as a high-power cathode material for lithium ion batteries. Nanoscale 3:4752–8
21. Yoo E, Kim J, Hosono E, Zhou H-S, Kudo T, Honma I (2008) Large reversible Li storage of graphene nanosheet families for use in rechargeable lithium ion batteries. Nano lett 8:2277–82
22. Wang X, Shi G (2015) Flexible graphene devices related to energy conversion and storage. Energy Environ Sci 8:790–823
23. Gwon H, Kim H-S, Lee KU, Seo D-H, Park YC, Lee Y-S, Ahn BT, Kang K (2011) Flexible energy storage devices based on graphene paper. Energy Environ Sci 4:1277–83
24. Yang S, Gong Y, Liu Z, Zhan L, Hashim DP, Ma L, Vajtai R, Ajayan PM (2013) Bottom-up approach toward single-crystalline VO_2-graphene ribbons as cathodes for ultrafast lithium storage. Nano Lett 13:1596–601
25. Zhang Y, Pan A, Liang S, Chen T, Tang Y, Tan X (2014) Reduced graphene oxide modified V_2O_3 with enhanced performance for lithium-ion battery. Mater Lett 137:174–7
26. Xu J, Li Z, Zhang X, Huang S, Jiang S, Zhu Q, Sun H, Zakharova GS (2014) Self-assembled V_3O_7/graphene oxide nanocomposites as cathode material for lithium-ion batteries. Int J Nanotech 11:808–18
27. Wang H, Cui L-F, Yang Y, Casalongue HS, Robinson JT, Liang Y, Cui Y, Dai H (2010) Mn_3O_4-graphene hybrid as a high-capacity anode material for lithium ion batteries. J Am Chem Soc 132:13978–80
28. Perera SD, Liyanage AD, Nijem N, Ferraris JP, Chabal YJ, Balkus KJ (2013) Vanadium oxide nanowire—graphene binder free nanocomposite paper electrodes for supercapacitors: a facile green approach. J Power Sources 230:130–7
29. Pan GX, Xia XH, Cao F, Chen J, Zhang YJ (2014) Carbon cloth supported vanadium pentaoxide nanoflake arrays as high-performance cathodes for lithium ion batteries. Electrochimi Acta 149:349–54
30. Ramana CV, Smith RJ, Hussain OM, Massot M, Julien CM (2005) Surface analysis of pulsed laser-deposited V_2O_5 thin films and their lithium intercalated products studied by Raman spectroscopy. Surface Interface Analy 37:406–11
31. Qin M, Liang Q, Pan A, Liang S, Zhang Q, Tang Y, Tan X (2014) Template-free synthesis of vanadium oxides nanobelt arrays as high-rate cathode materials for lithium ion batteries. J Power Sources 268:700–5
32. Liang S, Hu Y, Nie Z, Huang H, Chen T, Pan A, Cao G (2015) Template-free synthesis of ultra-large V_2O_5 nanosheets with exceptional small thickness for high-performance lithium-ion batteries. Nano Energy 13:58–66
33. Braithwaite JS, Catlow CRA, Gale JD, Harding JH (1999) Lithium intercalation into vanadium pentoxide: a theoretical study. Chem Mater 11:1990–8
34. Su J, Wu X-L, Lee J-S, Kim J, Guo Y-G (2013) A carbon-coated $Li_3V_2(PO_4)_3$ cathode material with an enhanced high-rate capability and long lifespan for lithium-ion batteries. J Mater Chem A 1:2508

35. Zhang C, Chen Z, Guo Z, Lou XW (2013) Additive-free synthesis of 3D porous V_2O_5 hierarchical microspheres with enhanced lithium storage properties. Energy Environ Sci 6:974–8
36. Wang S, Li S, Sun Y, Feng X, Chen C (2011) Three-dimensional porous V_2O_5 cathode with ultra high rate capability. Energy Environ Sci 4:2854
37. Su YH, Pan AQ, Wang YP, Huang JW, Nie ZW, An XX, Liang SQ (2015) Template-assisted formation of porous vanadium oxide as high performance cathode materials for lithium ion batteries. J Power Sources 295:254–258
38. Chou SL, Wang JZ, Sun JZ, Wexler D, Forsyth M, Liu HK, Dou SX (2008) High capacity, safety, and enhanced cyclability of lithium metal battery using a V_2O_5 nanomaterial cathode and room temperature ionic liquid electrolyte. Chem Mater 20(22):7044–7051
39. Zhang YF, Pan AQ, Wang YP, Wei WF, Su YH, Hu JM, Liang SQ (2016) Dodecahedron-shaped porous vanadium oxide and carbon composite for high-rate lithium ion batteries. ACS Appl Mater Interfaces 8(27):17303–17311